Dispersive line shapes and optical pumping in a three-level system

Matti Kaivola,* Per Thorsen, and Ove Poulsen
Institute of Physics, University of Aarhus, DK-8000 Aarhus C, Denmark
(Received 14 January 1985)

Dispersive line shapes have been observed in the population of the intermediate level of a three-level Λ configuration in a fast beam of metastable $^{40}Ca^*$ atoms. A steady-state calculation in the weak-probe approximation is used to identify the main physical processes in the interaction of the system with a weakly saturating pump field and a weak probe field. It is shown how optical-pumping effects between the lower levels can be used to select one particular two-photon process. The selection is enhanced by the narrow Doppler profile of the fast beam. Our simple analysis explains the resulting dispersive line shapes both qualitatively and quantitatively.

I. INTRODUCTION

One of the most extensively utilized schemes in nonlinear laser spectroscopy is the three-level configuration where two optical fields are in resonance with transitions sharing a common intermediate level. In spite of its seeming simplicity, this optical double-resonance problem has initiated an impressive number of both experimental and theoretical studies over the past 15 years.[1]

A characteristic feature that makes a three-level system such an interesting object of study is the induced two-photon coherence between the extreme levels that are not coupled directly by an electric dipole transition. In a Λ-type three-level configuration (Fig. 1), where the two lower levels can easily have very long lifetimes, the relaxation rate of the two-photon coherence may become extremely small, and consequently very sharp resonances may emerge in the response of the system to the applied optical fields. In such a system, the two-photon coherence couples to the single-photon coherences in such a way that at exact resonance, the system is efficiently pumped into a superposition state of the lower levels. In this state, the intermediate level is totally decoupled. The population is trapped to the lower levels, and no absorption to the intermediate level will take place.[2–12]

In the past few years, this phenomenon has achieved considerable interest, not the least because of its possible applications in building new frequency standards.[13–17] In this paper, we describe measurements that were done in a Λ configuration in a fast beam of Ca atoms (Fig. 1). One of the transitions was driven by a weakly saturating pump field with fixed detuning and the other by a copropagating weak probe field, the frequency of which was scanned over the resonances. The detected observable was the intermediate-level population.

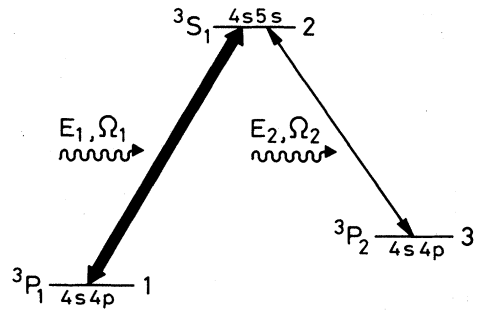

FIG. 1. The stronger laser acts on the transition $4s4p\ ^3P_1 - 4s5s\ ^3S_1$ (612.2 nm), the probe laser on the transition $4s4p\ ^3P_2 - 4s5s\ ^3S_1$ (616.3 nm). The metastable lower levels are populated in charge-exchange collisions of fast accelerated $^{40}Ca^+$ ions with sodium atoms. The intermediate-level lifetime is 10.7 ns. 35% of the relaxation of the intermediate level is directed to level 1, 53% to level 3.

The experimental configuration is well suited for studying the fundamental interaction processes in the system.[18] When both of the lower levels are initially populated, there are four fully coherent two-photon processes involved in the interaction of the system with the optical fields. Each of these processes leads to a narrow spectral structure. However, even at very modest pump-field intensities, optical pumping in the system will cause one of these processes to grow at the expense of the others. Depending on the frequency of the pump laser and as a function of the detuning of the probe laser, this process shows various dispersive and absorptive line shapes. Dispersive features in a Λ configuration have been discussed earlier, e.g., in Refs. 3, 4, 10, and 19.

After a description of the experimental apparatus and results in Sec. II, an analysis of the observed spectra, based on a density-matrix calculation in the weak probe approximation, is given (Sec. III). A similar analysis was earlier applied to a three-level ladder configuration of Ne atoms.[19]

II. EXPERIMENTAL

A. Apparatus

The experimental setup is shown in Fig. 2. Only the main characteristics of the apparatus are outlined in the following. A more detailed description can be found elsewhere.[20]

A beam of metastable $^{40}Ca^*$ atoms was produced by charge exchange of 100-keV $^{40}Ca^+$ ions in sodium vapor at a pressure of ~ 1 mTorr. After charge exchange, the atoms interacted with the two linearly polarized laser fields that were combined in a beam-splitting-type Glan-Thompson prism and were superimposed on the atomic beam in a colinear geometry. The interaction region was

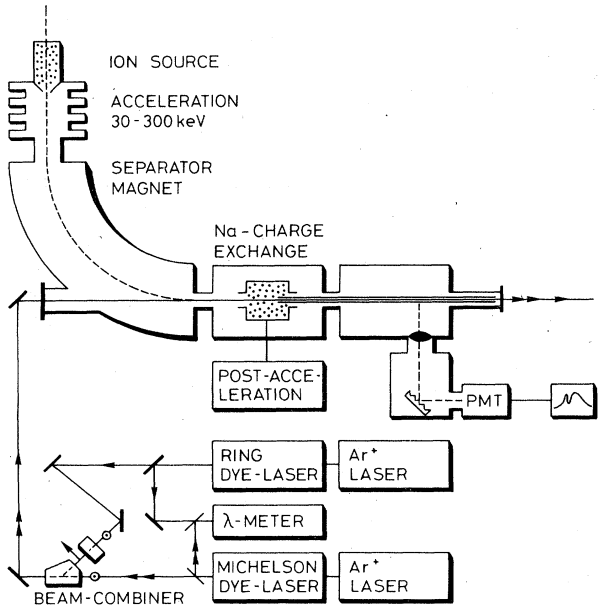

FIG. 2. Experimental setup.

shielded with a μ-metal tubing against external magnetic fields. Approximately 1 m downstream in the beam, the intermediate-level population was detected by observing fluorescence from this level down to level 3 in a direction perpendicular to the beam.

The weakly saturating pump field acting on the transition from level 1 to level 2 was provided by a double-Michelson dye laser[21] that was actively stabilized to an external optical cavity by using the polarization spectroscopy scheme of Hansch and Couillaud.[22] The intensity of the laser was typically 100 mW/cm^2 and the short-term frequency stability better than 100 kHz. A ring-dye laser was used as the probe laser with a linewidth of $\lesssim 1$ MHz and with an intensity that was attenuated before the interaction to a level less than 1 mW/cm^2.

The width of the compressed velocity distribution of the fast beam was found by observing fluorescence from level 2 when the pump laser was turned off, and the probe laser was scanned across the $3\leftrightarrow 2$ resonance. The full width half maximum (FWHM) of the line was measured to be 44 MHz. The line was analyzed as a convolution of a Gaussian velocity profile and a Lorentzian homogeneous line with FWHM of 14.5 MHz, and a full width of 40 MHz for the velocity profile was found. This corresponds to a stability of the acceleration voltage of ± 3 V.

B. Experimental spectra

Typical experimental spectra are shown in Fig. 3. The pump laser was set at a fixed detuning from the exact resonance, and the probe laser was scanned over the $3\leftrightarrow 2$ resonance. At close to zero detuning of the pump laser, the width (FWHM) of the observed power-broadened nonabsorbing resonance was 4 MHz. When the pump-field intensity was attenuated to the same level as the probe, the line width was reduced to 1.5 MHz, now mainly determined by the uncorrelated frequency fluctuations of the two lasers.[11] To our knowledge, this represents the highest optical resolution so far obtained in a colinear fast-beam geometry.

When the pump laser was tuned slightly off from exact resonance, a sharp feature could still be observed in the fluorescence spectrum at a probe-laser detuning that corresponded to the pump-laser detuning. However, dramatic changes in the line shape of the narrow resonance could be seen as a function of the detuning. The line changed from an asymmetric dip at small detunings, through a purely dispersive shape, to an asymmetric peak at large values of the pump-laser detuning.

III. ANALYSIS OF THE Λ CONFIGURATION

A. Physical model

We describe the dynamics of the three-level system in the density-matrix formalism and write the equations of motion for the density-matrix elements in the rotating-wave approximation in the form

$$\dot{\rho}_{11}=-\gamma_1\rho_{11}+\Gamma_{21}\rho_{22}+2\mathrm{Im}(\alpha\tilde{\rho}_{21}) , \tag{1a}$$

$$\dot{\rho}_{22}=-\gamma_2\rho_{22}-2\mathrm{Im}(\alpha\tilde{\rho}_{21}+\beta\tilde{\rho}_{23}) , \tag{1b}$$

$$\dot{\rho}_{33}=-\gamma_3\rho_{33}+\Gamma_{23}\rho_{22}+2\mathrm{Im}(\beta\tilde{\rho}_{23}) , \tag{1c}$$

$$\dot{\tilde{\rho}}_{21}=-id_{21}\tilde{\rho}_{21}+i\alpha(\rho_{22}-\rho_{11})-i\beta\tilde{\rho}_{31} , \tag{1d}$$

$$\dot{\tilde{\rho}}_{23}=-id_{23}\tilde{\rho}_{23}+i\beta(\rho_{22}-\rho_{33})-i\alpha\tilde{\rho}^*_{31} , \tag{1e}$$

$$\dot{\tilde{\rho}}_{31}=-id_{31}\tilde{\rho}_{31}+i\alpha\tilde{\rho}^*_{23}-i\beta\tilde{\rho}_{21} , \tag{1f}$$

$$\tilde{\rho}_{ij}=\tilde{\rho}^*_{ji} . \tag{1g}$$

Two monochromatic laser fields with arbitrarily large amplitudes E_1 and E_2 are assumed to induce transitions with Rabi frequencies $\alpha=\mu_{12}E_1/2\hbar$ and $\beta=\mu_{32}E_2/2\hbar$, where μ_{12} and μ_{32} are the appropriate dipole-matrix elements of the transitions. The relaxation rate γ_k describes the decay of the level-k population and Γ_{kl} the spontaneous back coupling from level k to level l.

Since the velocities of the atoms are concentrated in a very narrow distribution around the average velocity V of the fast beam ($V\sim 10^{-3}c$), it is convenient to perform the calculation in a frame moving at the velocity V relative to the laboratory coordinate system. In this frame, the complex detuning parameters in Eqs. (1d)—(1f) are defined by

$$d_{kl}=\tilde{\Delta}_{kl}-i\gamma_{kl} , \tag{2}$$

where the Doppler-shifted detunings are

$$\tilde{\Delta}_{21}=\Delta_{21}+k_1v , \tag{3a}$$

$$\tilde{\Delta}_{23}=\Delta_{23}+k_2v , \tag{3b}$$

$$\tilde{\Delta}_{31}=\Delta_{31}+(k_1-k_2)v , \tag{3c}$$

and

$$\Delta_{21}=\omega_{21}-\Omega_1 , \tag{4a}$$

$$\Delta_{23}=\omega_{23}-\Omega_2 , \tag{4b}$$

$$\Delta_{31}=\Delta_{21}-\Delta_{23} . \tag{4c}$$

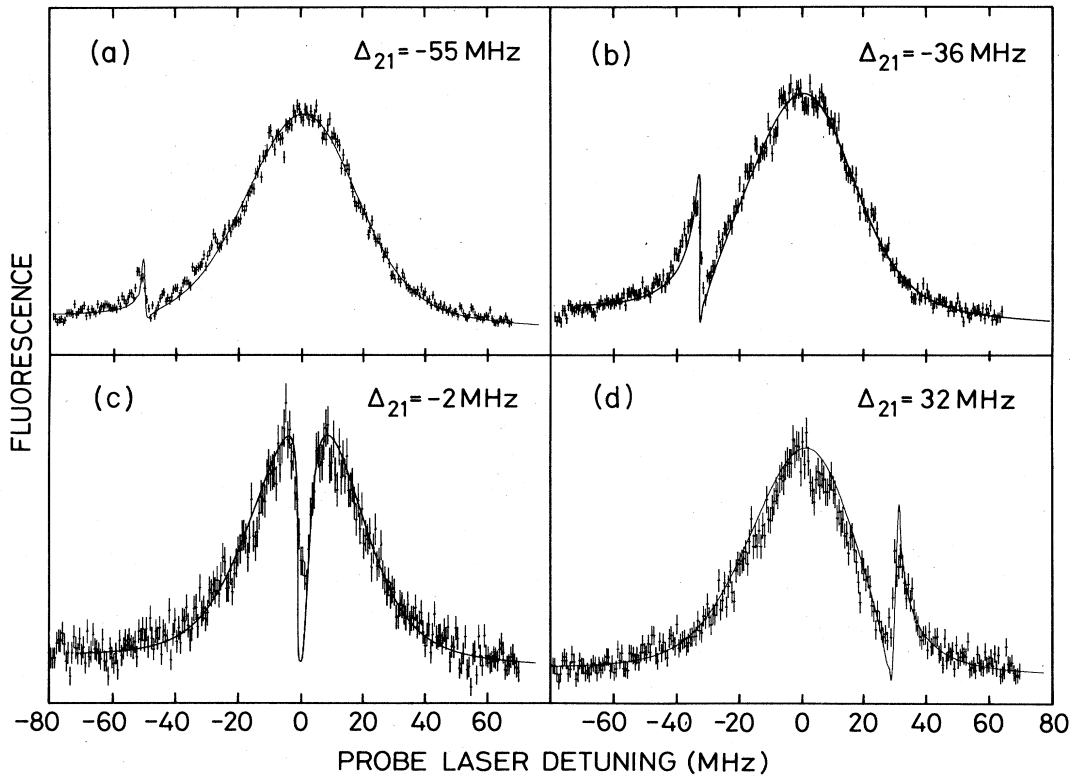

FIG. 3. Experimental spectra with four different pump-laser detunings $\Delta_{21}=-55$, -36, -2, and $+32$ MHz. The signal is the fluorescence from the intermediate level as a function of the probe-laser detuning Δ_{23}. In all the spectra, the Rabi frequency of the pump laser was $\alpha=40/2\pi$ MHz and that of the probe laser $\beta=5/2\pi$ MHz. The solid curves are the results of simulations based on the steady-state density-matrix calculations [Eq. (6)] with experimental parameter values. Only the amplitude of the broad Voigt profile has been scaled in the simulations to approximately fit the experimental amplitude. No other fitting of the parameters has been performed.

Here Ω_1 and Ω_2 are the laser frequencies in the moving frame, ω_{21} and ω_{23} the resonance frequencies of the atom, v the atomic velocity relative to the moving frame ($v \ll V$), and $k_{1,2}=\Omega_{1,2}/c$. If the laser frequencies in the laboratory frame are $\Omega^L_{1,2}$, then

$$\Omega_{1,2}=\Omega^L_{1,2}(1-V/c)/\sqrt{1-V^2/c^2}\,. \tag{5}$$

Since no collisions take place in the fast beam, no incoherent pumping of the populations occurs, and the relaxation rates of the coherences satisfy $\gamma_{kl}=\frac{1}{2}(\gamma_k+\gamma_l)$.

The set of the nine linear-coupled homogeneous differential equations with constant coefficients can readily be solved numerically,[6,11] with the initial condition that only the matrix elements ρ_{11} and ρ_{33} are nonzero at $t=0$ [$\rho_{11}(0)=n^0_1$ and $\rho_{33}(0)=n^0_3$]. The problem reduces to finding the nine eigenvalues and eigenvectors of the complex coefficient matrix. This task even a small computer can handle reasonably fast, but when the averaging over the velocities is included, the computation time increases drastically.

However, it will turn out that a steady-state version of the theory, with the additional assumption that the probe beam is weak, suffices to reproduce the experimental results. Finally, to identify the physical features, we go to the limit where both beams are assumed weak.

B. Steady-state approximation

In the experiment, the intermediate-level population is observed after an interaction time of $\tau=1.2$ μs. In this time, all rapid initial transients have died out, and an approximately stationary state corresponding to the population remaining in the system has been reached. Of course, since the intermediate level is continuously leaking out of the system, the level populations will never reach true ensemble-averaged steady-state values in the beam experiment, except for the special case when population trapping occurs, and the leaking level is totally decoupled from the system. However, in this particular experimental case, the leak is relatively slow, only 12% of the intermediate-level relaxation is directed out. Thus the steady-state solution of Eqs. (1a)—(1g) is expected to give a good account of the experiment.

To find the steady-state solution, we set the left-hand-side derivatives of Eqs. (1a)—(1f) equal to zero and include a pumping term for the initially populated levels 1 and 3 in Eqs. (1a) and (1c). This pumping describes the entrance of the atoms to the interaction region, and it is taken to be

$\lambda_1=n_1^0\gamma_1$ and $\lambda_3=n_3^0\gamma_3$, so that when no fields are present, the level populations are $\rho_{11}=n_1^0$, $\rho_{22}=0$, and $\rho_{33}=n_3^0$.

The effect of the long but still finite interaction time of the atoms and the fields is approximated by introducing an exponential-decay rate $1/\tau$ into the steady-state equations. Since $\gamma_1,\gamma_3 \ll 1/\tau \ll \gamma_2$, this is with good accuracy equivalent to replacing the essentially zero relaxation rates of the lower states γ_1 and γ_3, by $1/\tau$.

C. Weak probe approximation

The resulting set of algebraic equations can be solved analytically.[1] However, since one of the fields is a weak probe, much more insight into the nature of the solution is gained by going to the perturbation limit and by treating one of the Rabi frequencies as a small parameter. After a straightforward but tedious calculation, the solution of ρ_{22} to all orders in α^2 and to the lowest order in β^2 is found to be

$$\rho_{22}=\rho_{22}^{(0)}-\frac{2\beta^2}{\gamma_2}(\rho_{33}^{(0)}-\rho_{22}^{(0)})\left[1+\left[\frac{\Gamma_{21}}{\gamma_1}-1\right]\frac{\rho_{22}^{(0)}}{n_1^0}\right]\mathrm{Im}\left[\frac{1}{d_{23}^*}\right] \tag{6a}$$

$$+\frac{2\alpha^2\beta^2}{\gamma_2}(\rho_{33}^{(0)}-\rho_{22}^{(0)})\left[1+\left[\frac{\Gamma_{21}}{\gamma_1}-1\right]\frac{\rho_{22}^{(0)}}{n_1^0}\right]\mathrm{Im}\left[\frac{1}{d_{23}^*(d_{23}^*d_{31}+\alpha^2)}\right] \tag{6b}$$

$$-\frac{2\alpha^2\beta^2}{\gamma_2}\left\{(\rho_{11}^{(0)}-\rho_{22}^{(0)})\left[1+\left[\frac{\Gamma_{21}}{\gamma_1}-1\right]\frac{\rho_{22}^{(0)}}{n_1^0}\right]\right.$$

$$\left.+(\rho_{33}^{(0)}-\rho_{22}^{(0)})\left[1-\frac{(\gamma_1+\gamma_2-\Gamma_{21})}{\gamma_1}\frac{\rho_{22}^{(0)}}{n_1^0}\right]\right\}\mathrm{Im}\left[\frac{1}{d_{21}(d_{23}^*d_{31}+\alpha^2)}\right] \tag{6c}$$

$$+\frac{2\alpha^2\beta^2}{\gamma_2}(\rho_{11}^{(0)}-\rho_{22}^{(0)})\left[1-\frac{(\gamma_1+\gamma_2-\Gamma_{21})}{\gamma_1}\frac{\rho_{22}^{(0)}}{n_1^0}\right]\mathrm{Im}\left[\frac{d_{23}^*}{d_{21}^2(d_{23}^*d_{31}+\alpha^2)}\right], \tag{6d}$$

where $\rho_{kk}^{(0)}$ are the steady-state populations when only the strong field is acting ($\beta^2=0$),

$$\rho_{11}^{(0)}=n_1^0-\frac{1}{\gamma_1}(\gamma_2-\Gamma_{21})\rho_{22}^{(0)}, \tag{7a}$$

$$\rho_{22}^{(0)}=n_1^0\frac{2\alpha^2\gamma_{21}}{\gamma_2(\tilde{\Delta}_{21}^2+\Gamma^2)}, \tag{7b}$$

$$\rho_{33}^{(0)}=n_3^0+\frac{\Gamma_{23}}{\gamma_3}\rho_{22}^{(0)}, \tag{7c}$$

and

$$\Gamma^2=\gamma_{21}^2+\frac{2\alpha^2\gamma_{21}}{\gamma_1\gamma_2}(\gamma_1+\gamma_2-\Gamma_{21}). \tag{8}$$

Figure 3 shows a comparison between the experimental spectra and the numerically velocity-averaged steady-state simulations of the intermediate-level population ρ_{22} from Eq. (6).[23] In the simulations, experimental values for the relaxation rates, Rabi frequencies, and the width of the Gaussian velocity profile were used. In Fig. 3, the height of the broad feature in the simulations has been approximatively scaled to the corresponding experimental one. We stress that no other parameter has been adjusted. The only parameter that differs between the spectra is the experimental pump-laser detuning Δ_{21}.

The steady-state model is seen to reproduce the essential features of the experimental spectra satisfactorily. Smearing of the narrow spectral features due to uncorrelated frequency fluctuations of the lasers explains the differences between the simulations and the experimental spectra at the $\lesssim$1-MHz level. In the scale of Figs. 3(a)—3(d), the time-dependent solution was found to be indistinguishable from the steady-state version.

D. Main physical processes

The underlying main physical processes in the solution for the population ρ_{22} [Eq. (6)] can be identified by going to the lowest-order limit in the Rabi frequencies of both fields.[19,24] Preserving terms only to the first order in α^2 in the power series expansion of Eq. (6), we obtain

$$\rho_{22}=\rho_{22}^{\mathrm{RE}} \tag{9a}$$

$$+\frac{2\alpha^2\beta^2}{\gamma_2}n_3^0\mathrm{Im}\left[\frac{1}{(d_{23}^*)^2 d_{31}}\right] \tag{9b}$$

$$-\frac{2\alpha^2\beta^2}{\gamma_2}(n_1^0+n_3^0)\mathrm{Im}\left[\frac{1}{d_{21}d_{23}^*d_{31}}\right] \tag{9c}$$

$$+\frac{2\alpha^2\beta^2}{\gamma_2}n_1^0\mathrm{Im}\left[\frac{1}{d_{21}^2 d_{31}}\right] \tag{9d}$$

where

$$\rho_{22}^{\mathrm{RE}}=\frac{2\alpha^2}{\gamma_2}n_1^0\mathrm{Im}\left[\frac{1}{d_{21}}\right]+\frac{2\beta^2}{\gamma_2}n_3^0\mathrm{Im}\left[\frac{1}{d_{23}}\right]$$
$$+\frac{2\alpha^2}{\gamma_2}\frac{2\beta^2}{\gamma_2}\left[\left[n_1^0\frac{\Gamma_{23}}{\gamma_3}+n_3^0\frac{\Gamma_{21}}{\gamma_1}\right]-(n_1^0+n_3^0)\right]$$
$$\times\mathrm{Im}\left[\frac{1}{d_{21}}\right]\mathrm{Im}\left[\frac{1}{d_{23}}\right]. \tag{10}$$

The rate-equation contribution ρ_{22}^{RE} describes the pure population effects which include the two single-photon transitions from the lower levels to the common intermediate level and their cross terms that correspond to the stepwise transitions between the levels. The stepwise term includes positive contributions from processes where one field first induces the transition $1\leftrightarrow 2$ ($2\leftrightarrow 3$), then the system spontaneously decays to 3 (1), and finally, the other field induces the transition $3\leftrightarrow 2$ ($1\leftrightarrow 2$). The negative terms are due to hole burning. However, in the present case, when $\Gamma_{21}/\gamma_1,\Gamma_{23}/\gamma_3\gg 1$, the hole burning is negligible.

After integration over the Gaussian velocity distribution of the atoms, the first term in ρ_{22}^{RE} just gives a constant background contribution to the intermediate-level population. When expressed as a function of the scanned-laser frequency Ω_2^L, the second term adds a Doppler-broadened feature on top of this background. Since the homogeneous linewidth starts to be of the same order of magnitude as the Doppler width, 14.5 and 40 MHz, respectively, the line shape of this second term will not be a pure Gaussian but really a Voigt profile. For the same reason, it is difficult to distinguish the small stepwise contribution on top of this Voigt profile.

The qualitative picture of the role of the pure population effects on the steady-state population of the intermediate level holds true also when the Rabi frequency of the fixed-frequency pump laser is taken into account to all orders as in Eq. (6).

The interesting part of Eq. (9) is the group of the last three terms, describing the fully coherent contributions of ρ_{22} to the lowest order. The physical processes behind them can be identified by looking at the coherences included in the different terms. Neglecting the difference between the complex conjugate quantities, the second of these coherent terms, (9c), is found to be a sum of two symmetrical processes starting from levels 1 and 3, respectively,

$$\rho_{11}\overset{\alpha}{\rightarrow}\tilde{\rho}_{12}\overset{\beta}{\rightarrow}\tilde{\rho}_{31}\overset{\alpha}{\rightarrow}\tilde{\rho}_{23}\overset{\beta}{\rightarrow}\rho_{22}, \tag{11a}$$

$$\rho_{33}\overset{\beta}{\rightarrow}\tilde{\rho}_{23}\overset{\alpha}{\rightarrow}\tilde{\rho}_{31}\overset{\beta}{\rightarrow}\tilde{\rho}_{12}\overset{\alpha}{\rightarrow}\rho_{22}. \tag{11b}$$

The coherent terms (9b) and (9d) are identified as their twin processes where the time ordering of the two last interactions has been interchanged with respect to (11a) and (11b),

$$\rho_{33}\overset{\beta}{\rightarrow}\tilde{\rho}_{23}\overset{\alpha}{\rightarrow}\tilde{\rho}_{31}\overset{\alpha}{\rightarrow}\tilde{\rho}_{23}\overset{\beta}{\rightarrow}\rho_{22}, \tag{11c}$$

$$\rho_{11}\overset{\alpha}{\rightarrow}\tilde{\rho}_{21}\overset{\beta}{\rightarrow}\tilde{\rho}_{31}\overset{\beta}{\rightarrow}\tilde{\rho}_{21}\overset{\alpha}{\rightarrow}\rho_{22}. \tag{11d}$$

Processes (11a)—(11d) describe all the four possible ways the coherences in the system can couple the populations of the lower levels to the intermediate-level population when each field is allowed to interact twice with the atoms.

It is interesting to note that in the case of equal zero-field populations of the lower levels, i.e., $n_1^0=n_3^0$, each of the coherent two-photon processes (11a)—(11d) behaves in this lowest-order approximation formally like a two-level resonance from the appropriate lower level to the intermediate level but with an effective Rabi frequency that depends on the laser detunings. The other lower level is connected to this effective two-level system only through spontaneous decay from level 2. It should be noted that the square of the effective Rabi frequency may also be negative, and correspondingly negative transition rates may occur. For example, the square of the Rabi frequency connected to the process (11c) is

$$(\beta_{\mathrm{eff}})^2=\frac{\alpha^2\beta^2}{\gamma_{23}}\mathrm{Im}\left[\frac{d_{23}}{d_{23}^*d_{31}}\right], \tag{12}$$

which at exact resonance ($\Delta_{23}=\Delta_{31}=0$) becomes

$$(\beta_{\mathrm{eff}})^2=-\frac{\alpha^2\beta^2}{\gamma_{23}}\frac{1}{\gamma_{31}}. \tag{13}$$

In this picture, process (11c) describes a nonabsorbing resonance from level 3 to level 2 that creates a dip on the upper-level population and a peak on the lower-level population. The dip on level 2 decays spontaneously to level 1 with the rate Γ_{21}. A similar description can be given to all the other processes as well.

To determine the relative importance of the different coherent contributions to the intermediate-level population, we return to the result of Eq. (6) where only the probe field was assumed weak. It is noticed that the relative strengths of the processes (11a)—(11d) depend on the population differences exerted by the pump field. Since the coherent two-photon resonances are essentially velocity independent, the relative strengths can be qualitatively estimated by velocity averaging the factors in front of the line-shape functions. Figure 4 shows these factors as a function of the pump-transition Rabi frequency α for three different pump-laser detunings Δ_{21}.

Due to the very narrow Doppler width of a fast atomic beam, even a very modest Rabi frequency will pump the total population from level 1 to level 3 so effectively that process (11c) becomes the most important channel of coherent interaction.

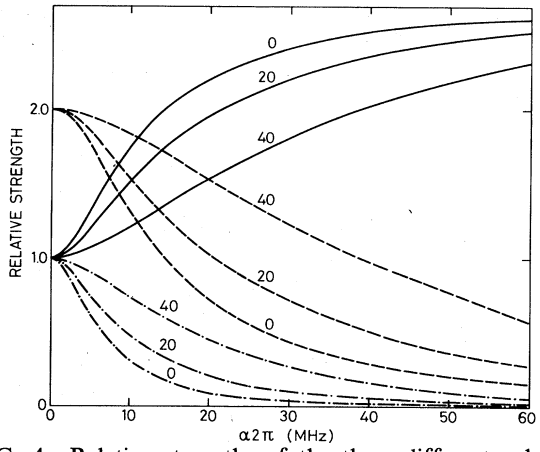

FIG. 4. Relative strengths of the three different coherent contributions of Eq. (6). The factors in front of the line-shape functions have been averaged over velocities and are plotted as functions of the pump-laser Rabi frequency α for three different pump-laser detunings $\Delta_{21}=0,20,40$ MHz. Both lower levels are assumed to be equally populated at zero fields, $n_1^0=n_3^0$. —— corresponds to term (6b), — — — to term (6c), and —·—·—· to term (6d).

The velocity-averaged contributions of the three fully coherent terms of Eq. (6) are shown in Fig. 5 as a function of the probe-laser detuning. Each contribution is plotted for six different pump-laser detunings and for three different pump-transition Rabi frequencies. The curves of Fig. 5 show that the first coherent term, term (6b), clearly gives the main contribution at the Rabi frequency $\alpha=40/2\pi$ MHz. The arguments given above about the relative strengths of the possible processes are thus verified.

When the fixed pump laser is tuned to exact resonance, this term gives a narrow dip at $\Delta_{23}=0$. When the pump laser is detuned, the line shape first becomes dispersive, and at large values of Δ_{21}, it goes over to a positive peak. This behavior can qualitatively be seen again by going to the lowest order in both Rabi frequencies since increasing α mainly affects the line shape only by broadening it, as seen in Fig. 5. In this lowest-order approximation, the line-shape function of process (11c) can be written as a sum of three terms

$$\mathrm{Im}\left[\frac{1}{(d_{23}^{*})^2 d_{31}}\right]=-2\mathscr{D}(31)[\mathscr{D}(23)\mathscr{L}(23)] + \mathscr{L}(31)[\mathscr{D}(23)^2-\mathscr{L}(23)^2]\,, \tag{14}$$

where we have defined

$$\mathscr{L}(kl)=\gamma_{kl}/(\Delta_{kl}^2+\gamma_{kl}^2) \tag{15}$$

and

$$\mathscr{D}(kl)=\Delta_{kl}/(\Delta_{kl}^2+\gamma_{kl}^2)\,. \tag{16}$$

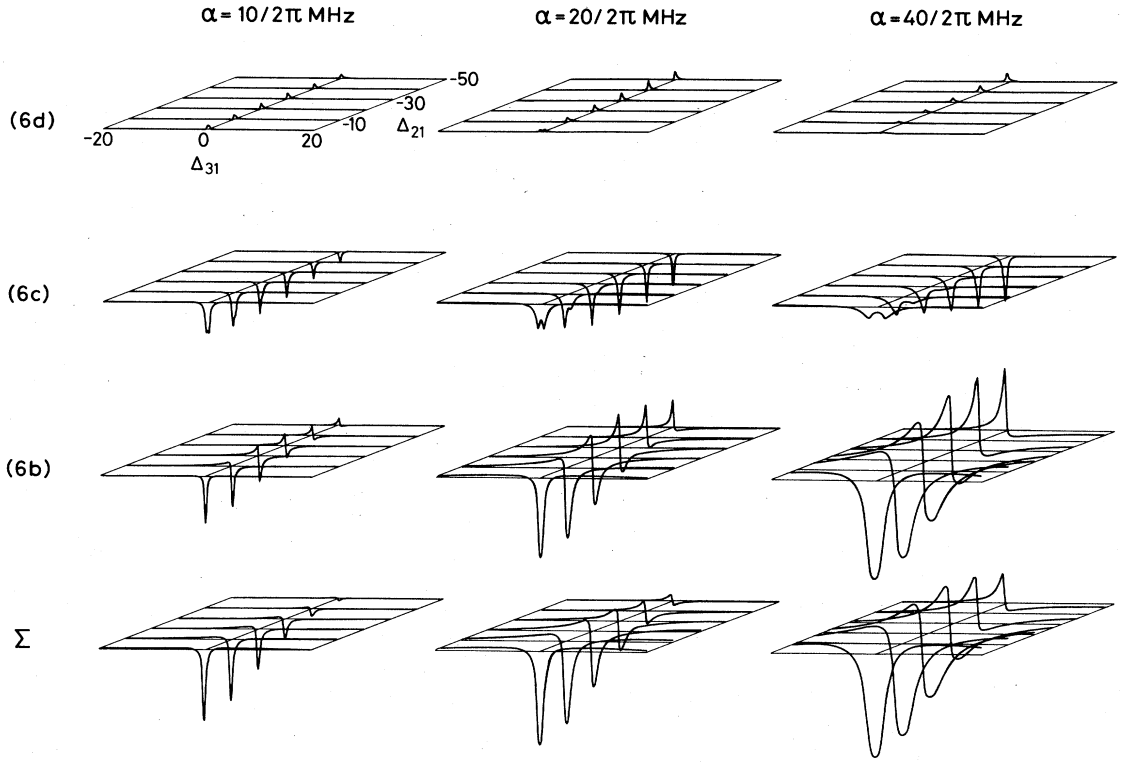

FIG. 5. The velocity-averaged contributions from the three fully coherent terms (6b)—(6d) and their sum as a function of the two-photon detuning $\Delta_{31}=\Delta_{21}-\Delta_{23}$ (in MHz) for six different pump-laser detunings $\Delta_{21}=0$, -10, -20, -30, -40, and -50 MHz. Each contribution has been plotted for three different pump-transition Rabi frequencies, $\alpha=10/2\pi$, $20/2\pi$, and $40/2\pi$ MHz.

When the Doppler integral is made, the functions $\mathscr{D}(31)$ and $\mathscr{L}(31)$ which do not essentially depend on the velocity, give narrow resonance structures around $\Delta_{31}=\Delta_{21}-\Delta_{23}\simeq 0$. Thus, the first term of Eq. (14) leads to a dispersive contribution, while the second and third terms give positive- and negative-going peaks, respectively. The relative weights of these structures are determined by the Doppler integrals of the manifestly velocity-dependent factors in Eq. (14), and they depend parametrically on the fixed detuning of the pump laser, Δ_{21}, through the resonance condition $\Delta_{21}\simeq\Delta_{23}$. At small detunings Δ_{21}, the largest weight originates from the third term of Eq. (14), and a negative-going dip in the population of level 2 as a function of the probe-laser frequency emerges. At large detunings Δ_{21}, the second term becomes the largest, and a positive peak is observed. For a detuning Δ_{21} such that the velocity integrals of $\mathscr{D}(23)^2$ and $\mathscr{L}(23)^2$ are equal, the line shape is purely dispersive. This occurs when the pump laser is tuned approximately half the Doppler width away from the exact resonance.

IV. CONCLUDING REMARKS

Although our experimental configuration clearly calls for a time-dependent solution of the density-matrix equations in a general case, the studied Λ configuration in Ca could be treated within the experimental accuracy by using the steady-state approximation. Also, since one of the fields was a weak probe, further simplification and more physical insight in the model could be achieved by treating the weak-field Rabi frequency as a small parameter in a perturbation calculation. These approximations made it possible to identify the main physical interaction processes.

In a three-level system, the one- and two-photon coherences can interfere in a complicated manner. However, the analysis showed that the optical-pumping effect of the stronger field favors one of the four possible, coherent, two-photon processes. This process differs in the time ordering of the last two interactions with the fields from the type of two-photon process that gives the "normal" coherent, two-photon absorption in a three-level ladder configuration. The narrow Doppler width of the optical transitions in a fast atomic beam greatly enhances the optical pumping and thus conveniently allows this particular process to be separated from the other processes involved. At certain detunings, this process leads to very sharp, purely dispersive line shapes, in agreement with the experimental observations.

As stated, in the experiment, use was made of the velocity compression occurring in a fast beam. Recently, narrow Doppler profiles have been produced also by laser cooling of trapped ions.[25] Similar spectral structures as described in this paper are then expected to be observable in spectroscopic studies of the same type of configurations in trapped, cold ions, too.

ACKNOWLEDGMENTS

The authors wish to thank Dr. J. Javanainen for a critical reading of the manuscript, and U. Nielsen for assistance with the computer calculations. This work was financially supported by the Academy of Finland and the Carlsberg Foundation.

---

*Permanent address: Helsinki University of Technology, Department of Technical Physics, SF-02150 Espoo 15, Finland.

[1]An excellent list of general references to three-level spectroscopy can be found in, e.g., C. Feuillade and P. R. Berman, Phys. Rev. A **29**, 1236 (1984).

[2]G. Alzetta, A. Gozzini, L. Moi, and G. Orriols, Nuovo Cimento B **36**, 5 (1976).

[3]E. Arimondo and G. Orriols, Lett. Nuovo Cimento **17**, 333 (1976).

[4]G. Alzetta, L. Moi, and G. Orriols, Nuovo Cimento B **52**, 209 (1979).

[5]G. Orriols, Nuovo Cimento B **53**, 1 (1979).

[6]R. M. Whitley and C. R. Stroud, Jr., Phys. Rev. A **14**, 1498 (1976).

[7]H. R. Gray, R. M. Whitley, and C. R. Stroud, Jr., Opt. Lett. **3**, 218 (1978).

[8]D. E. Murnick, M. S. Feld, M. M. Burns, T. U. Kühl, and P. G. Pappas, *Laser Spectroscopy IV,* edited by H. Walther and K. W. Rothe (Springer, Berlin, 1979), p. 195.

[9]F. T. Hioe and J. H. Eberly, Phys. Rev. Lett. **47**, 839 (1981).

[10]P. M. Radmore and P. L. Knight, J. Phys. B **15**, 561 (1982).

[11]B. J. Dalton and P. L. Knight, J. Phys. B **15**, 3997 (1982).

[12]S. Swain, J. Phys. B **15**, 3405 (1982).

[13]R. P. Hackel and S. Ezekiel, Phys. Rev. Lett. **42**, 1736 (1979).

[14]J. E. Thomas, S. Ezekiel, C. C. Leiby, Jr., R. H. Picard, and C. R. Willis, Opt. Lett. **6**, 298 (1981).

[15]R. E. Tench, B. W. Peuse, P. R. Hemmer, J. E. Thomas, S. Ezekiel, C. C. Leiby, Jr., R. H. Picard, and C. R. Willis, J. Phys. (Paris) Colloq. **42**, C8-45 (1981).

[16]J. E. Thomas, P. R. Hemmer, S. Ezekiel, C. C. Leiby, Jr., R. H. Picard, and C. R. Willis, Phys. Rev. Lett. **48**, 867 (1982).

[17]P. Knight, Nature **297**, 16 (1982).

[18]P. E. Toschek, in *Frontiers in Laser Spectroscopy, Les Houches Session XXVII,* edited by R. Balian, S. Haroche, and S. Liberman (North-Holland, Amsterdam, 1977), p. 323.

[19]M. Kaivola, N. Bjerre, O. Poulsen, and J. Javanainen, Opt. Commun. **49**, 418 (1984).

[20]O. Poulsen and N. I. Winstrup, Phys. Rev. Lett. **47**, 1522 (1981).

[21]M. Pinard, C. G. Aminoff, and F. Laloë, Appl. Phys. **15**, 371 (1978).

[22]T. W. Hansch and B. Couillaud, Opt. Commun. **35**, 441 (1980).

[23]The spectra calculated in the moving frame are transformed back to the laboratory frame by the transformation

$$\Delta_{kl}^{L}=\Delta_{kl}\sqrt{1-V^2/c^2}/(1-V/c)\ .$$

However, since $V/c\sim 10^{-3}$, we can take $\Delta_{kl}\simeq\Delta_{kl}^{L}$.

[24]S. Stenholm, *Foundations of Laser Spectroscopy* (Wiley, New York, 1984).

[25]See, e.g., P. E. Toschek, W. Neuhauser, and M. Hohenstatt, in *Coherence and Quantum Optics V,* edited by L. Mandel and E. Wolf (Plenum, New York, 1984), and references therein.